Finite Element Modeling of Thermal Effect on Airport Slabs

Chuanyue Shen, Yu Song, David Lange, Omar Jadallah, Jeffery Roesler

Department of Civil and Environmental Engineering, University of Illinois at Urbana-Champaign

ABSTRACT

A sub-ground tunnel connecting two concourses of a terminal at Chicago O'Hare International Airport suffered from water leakage. The airport engineers suspected that the problem was caused by high stresses impinging on the tunnel structure by the pavement sections above the tunnel, acting to damage joints and waterproofing membranes that should have prevented such leakage. To provide a fundamental solution to this problem while minimizing the interference with airport operation, a repair strategy needs to be determined based on a clear understanding of the root cause. A preliminary field inspection confirmed that the concrete pavement slabs moved significantly when ambient temperature changes caused concrete contraction or expansion. This study used finite element modeling to infer the slab displacements and stresses driven by the daily and seasonal thermal changes based on actual temperature statistics. We proposed a reasonable 3D model configuration for the entire pavement section. The simulated slab displacements agree with the results of actual manual measurements. Subsequent analysis predicts the stresses applied to the tunnel structure, whereby insightful data are obtained for preparing the repair plan.

1. INTRODUCTION

Chicago O'Hare International Airport (ORD) uses a sub-ground tunnel at Terminal 1 as a secure walkway connecting concourses B and C. The satellite image of this region is shown in Figure 1. A leak was found in the tunnel, allowing entry of water and deicing liquid runoff from the ground. It was suspected that high stresses, impinging on the tunnel structure by the pavement sections above the tunnel, caused the leak by acting to damage waterproofing joints and membranes. Concrete edge breakage, usually associated with high contact stresses, was observed near the expansion joints as shown in Figure 2. To provide a fundamental solution to this problem while minimizing the interference with airport operation, a repair strategy needs to be determined based on a clear understanding of the root cause.

Figure 1. Satellite image of Terminal 1 at ORD and outline of region of interest.

A preliminary field inspection confirmed that the concrete pavement slabs between concourses B and C moves significantly when ambient temperature changes cause concrete contraction or expansion. The slab movement was investigated via measuring the existing expansion joint opening near the tunnel.

The investigation showed that the joint displacement could exceed 50 mm (2 inches) over seasons. Soaring summer temperatures seemed to cause a complete closing of the joint. If the slab movement leads to stress buildup near the tunnel, the damage of the tunnel structure may occur.

Figure 2. Edge breakage at expansion joint between the tunnel and the slab

This study used finite element method (FEM) to investigate the movement of pavement slabs under the thermal influence. The major task is to simulate the stress buildup associated with joint displacement. The pavement section is reasonably

emulated using a simplified model configuration. A comparison between the simulation and the field inspection is conducted to valid the model performance. Subsequently, the influence of the joint width on the stress buildup in the tunnel is analyzed to inform the design of repair options.

2. MODEL CONFIGURATION

A 3D simulation is conducted in *Abaqus*^{TM}. The modeling process starts with geometry construction and meshing, followed by material property and boundary condition input. This section introduces the assumption and configuration of a base model.

The region of interest in the FEM analysis considered the concrete pavement section between the concourses B and C. The model geometry was generated using *AutoCAD®*, according to the satellite image. The concrete pavement section consists of thousands of small slab units, with a typical size of approximately 7.6 m by 7.6 m (25 ft by 25 ft). The depth was assumed as 1/20 of the side length, approximately 0.38 m (1.25 ft). The slab units were tied by dowel bars, such that it is reasonable to assume that the connected slabs move altogether. For simplicity, the small slab units were replaced with two large parts in the model, and the boundary structures were merged to one piece. The slab parts and the boundary structures are outlined in Figure 1 with yellow and red, respectively. In addition, a base was laid under the slab parts and boundary structures to simulate the ground.

The model configuration also accounted for the utility vaults that were found on slabs, as shown in Figure 3. They act as fixed points and induce constraints to the slabs, strongly influencing the overall responses. The utility vaults, shown as yellow dots in Figure 1, were included to the model according to their actual sizes and locations.
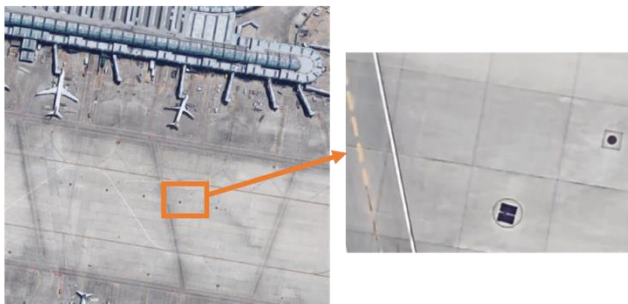
Figure 3. Utility vaults on the concrete slabs.

A gap opening was introduced to the south slab part to simulate the existing expansion joint that isolates the boundary structures from the outer concrete slabs. The joint is expected to reduce the stress concentration on the slabs and vary the slab movement. For comparison, the north slab part was left without gap opening. The joint width was assumed to be 500 mm to allow a full separation, and the sealant material was assumed to be silicon rubber.

The material properties of concrete and silicon rubber used in the study are based on engineering practices as in [1, 2, 3]. The material parameters are shown in Table 1.

The deformation mechanics and meshing types were assigned to the major parts of the model. The slab parts were designated as 3D deformable solid while the boundary structures and the ground as rigid body due to significant rigidity difference. The slab parts used C3D8 element type, and the others used R3D4. To optimize the overall simulation performance and consider the computational cost, the deformable slab parts were meshed finer while the rigid boundary and base coarser.

Simplified boundary conditions and contact methods were assigned to the model. The utility vaults were set as fixed boundary in which any movement was prohibited. The boundary structures and base were also fixed in place, restraining the movement of the slabs. The slab parts were only allowed to translation but not rotation. A hard contact mode was used for the interaction between the slab parts and the boundary structures. As such, the contact pressure was transferred only when they are in physical touch. No friction was assumed in the hard contact interface, but a reasonable Coulomb friction coefficient of 0.3 was assigned to the base. The self-weight of the concrete slabs was included in the model.

In terms of fulfilling the thermal change, we set different temperatures at different stages of the simulation. For example, we used two thermal steps to accomplish a complete temperature cycle of 20 ⁰C. The initial temperature was set to -5 ⁰C. The temperature at step 1 was set to 15 ⁰C to render an equivalent temperature rise of 20 ⁰C. At step 2, the temperature was set back to -5 ⁰C. With such a configuration, thermal stress can be simulated.

The model was solved using "Static, general" procedure in Abaqus/CAE with large-displacement formulation activated to handle potential nonlinear effect. The out-of-plane response was not considered in this analysis.

3. RESULT AND DISCUSSION OF THE MODEL

The outputs of slab displacement and stress distribution of the model are shown in Figure 4 to 7. The displacement map in Figure 4 shows that the slabs expand outward during temperature rise but are constrained by the fixed boundaries. The south slab part is only restrained by utility vaults, and it can deform freely at the edges due to the expansion joint. Compared with the south slab, the north slab part is more restrained since it has additional confinement from the boundary structures. When temperature drops, the slabs contract inward and leave small openings near the boundaries as a result of the ground friction.

Figure 5 shows the effective stress distribution. It is found that the stresses are concentrated at the utility vaults and the inner corners of the north slab during expansion, corresponding to the highly constrained positions in Figure 4. Additionally, there is negligible stress at free edges. After thermal contraction, residual stress is observed in the slabs, which confirms the influence of ground friction.

The confinement of the concourses and the tunnel influences the normal stress distributions in X and Y direction in Figures 6 and 7, respectively. The tensile stress is indicated in red and the compressive stress in blue. Comparing these two figures, it is noticed that the normal stress in Y direction is generally higher and has a larger coverage area than the normal stress in X direction. This observation indicates that the concourses have greater contribution to the confinement than the tunnel. In each figure, the south slab part shows less stress concentration than the north slab part, following the same trend found in the Figure 5.

The patterns of displacement and stress distribution are similar. A comparison between the south and north slab parts indicates that the joint can effectively release the constraint and greatly reduce the stress concentration. With the joint, the south slab part can reasonably simulate the realistic scenario.

In addition, the study assessed the accumulated effect of slab movement when undergoing several thermal cycles. This was investigated in a simplified case by implementing two temperature cycles of 20 ºC in the simulation. The accumulated maximum opening along the inner boundary is found to be 0.02 mm, which is small compared to the slab dimension. Thus, the accumulation has no essential effect on the overall slab movement.
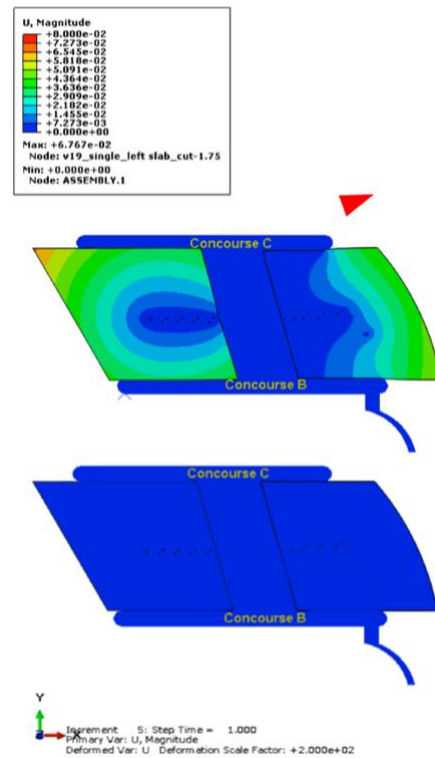
Figure 4. Displacement of the model with joint in south slab at (top) the highest temperature and (bottom) the lowest temperature, unit in meter.
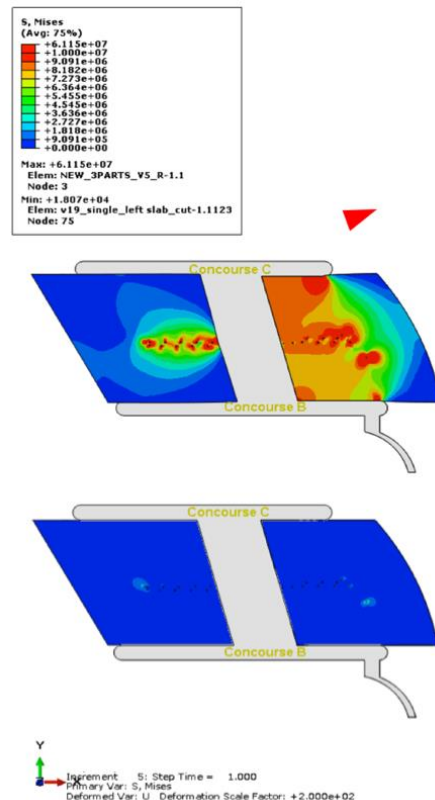
Figure 5. Effective stress distribution of the model with joint in south slab at (top) the highest temperature and (bottom) the lowest temperature, unit in Pascal.

3

4. VALIDATION OF MODEL PREDICTION

The validity of the model can be established by comparing the simulation results to the actual field manual measurements.

Two on-site inspections were conducted, and the average ambient temperature change was +10 ºC according to the weather report. We manually measured the joint openings along the tunnel expansion joints in the direction parallel to the concourses (X-direction in our model). In the simulation, the same temperature change of +10 ºC was used accordingly and the displacement map is shown in Figure 8.

The comparison focuses on six inspection locations that are highlighted with red dots in Figure 8. The comparison results are shown in Table 2. It is found that the simulated displacements in X direction of the six points are reasonably close to the field measurement. The overall higher displacement level in simulation can mainly associated with the joint width assumption, which allows a full separation at the tunnel boundary and eliminates the tunnel constraining effect on the slab movement. The field inspection also confirms the trend demonstrated in the simulation that the displacement appears smaller closer to the middle. Therefore, this simulation is proven to be solid and this model can predict the slab movement realistically.
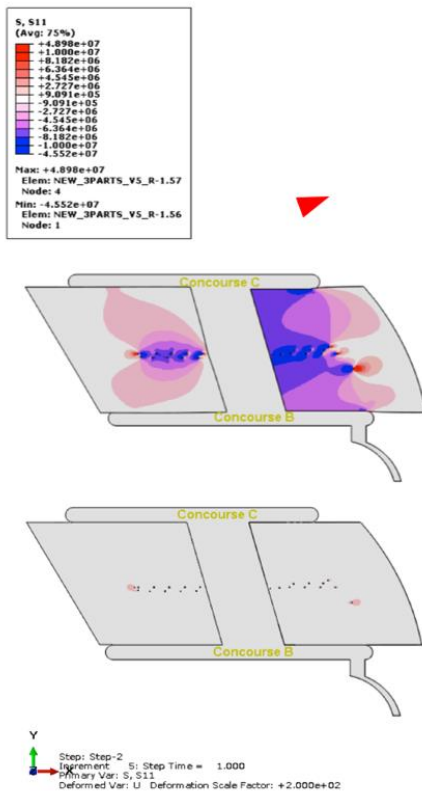
Figure 6. Normal stress distribution in X direction of the model with joint in south slab at (top) the highest temperature and (bottom) the lowest temperature, unit in Pascal.
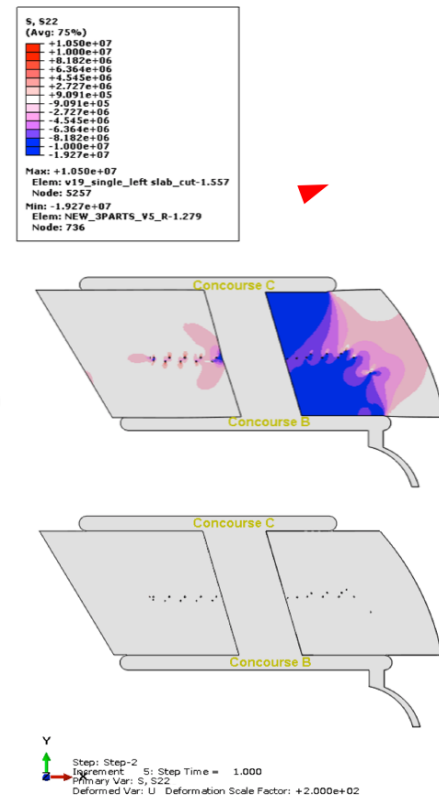
Figure 7. Y-normal stress distribution of the model with joint in south slab at (top) the highest temperature and (bottom) the lowest temperature, unit in Pascal.
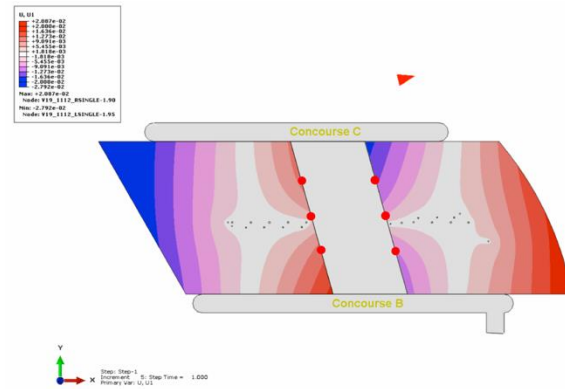
Figure 8. Displacement map in X direction of the model with joints in both slabs under 10 ºC temperature rise, unit in meter.

Table 1. Comparison of displacements in field and in model

	South (left)		North (right)	
	Field (mm)	Model (mm)	Field (mm)	Model (mm)
West (up)	4.39	9.51	10.02	13.70
Middle	6.78	4.04	5.60	5.31
East (down)	9.30	10.09	6.73	8.93

5. STRESS CONCENTRATION IN TUNNEL SLAB

The joint width affects the stress concentration in the tunnel slab, which may cause a damage near the boundary. This section compares three joint openings, i.e. 0, 20, and 30 mm, based on the validated model. The tunnel slab was set as deformable solid to reveal the stress.

Figure 9 shows the effective stress distributions in the tunnel slab. The maximum stress in tunnel slab is 3.608 MPa in the model without a join, which is sufficiently high to cause damage to the tunnel structure in a long term. In the 20-mm case, the maximum stress is greatly reduced to 1.285 MPa, which is only about 1/3 of the previous case. Concurrently, an overall reduction of the stress distribution is seen across most of the tunnel region. In the 30-mm case, the maximum stress is further reduced to 0.250 MPa. Evidently, stress concentration across the tunnel region is almost released. Assuming the tunnel is currently suffering from the worst-case scenario, an extra 30-mm cutoff along the expansion joint is recommended for the subsequent repair works to prevent reoccurrence of the tunnel damage in the future.

6. SUMMARY

This study utilized FEM simulation to understand the mechanism of observed slab movement at ORD concourses B and C and find a fundamental solution to resolve the distresses associated with the movement. Using actual geometry and ambient temperature data, the model reasonably simulated the realistic scenario. The model prediction reached a good agreement with the field manual measurement data. In a subsequent investigation, the joint width is confirmed to be critical to release the stress buildup in the tunnel region. For the subsequent repair work on the pavement section between the concourses, we suggest using an extra cutoff of 30-mm and above along the existing expansion joints to mitigate reoccurrences of the tunnel damage in the future.

Figure 9. Stress distribution of the tunnel slab in model with joint width of (top) 0, (middle) 20, and (bottom) 30 mm.

REFERENCES

1. Domone, P., Illston, J., 2010. Construction Materials: Their nature and behaviour 4th Ed. CRC Press.

2. Mindess, S., Young, F.J., Darwin, D., 2003. Concrete 2nd Ed. Upper Saddle River, NJ: Pearson Education, Inc.

3. AZO Materials. "Silicone Rubber". [Online]. Available: https://www.azom.com/properties.aspx?ArticleID=920.